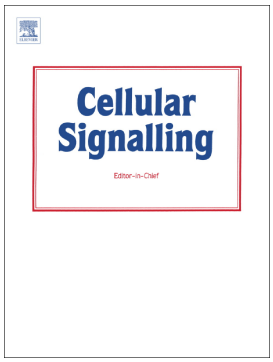

Metalloprotease ADAMTS-1 decreases cell migration and invasion modulating the spatiotemporal dynamics of Cdc42 activity

Maíra de Assis Lima, Suély Vieira da Silva, Orlando Serrano-Garrido, Maren Hülsemann, Luana dos Santos Neres, Juan Carlos Rodríguez-Manzaneque, Louis Hodgson, Vanessa M. Freitas

PII: S0898-6568(20)30304-1

DOI: https://doi.org/10.1016/j.cellsig.2020.109827

Reference: CLS 109827

To appear in: *Cellular Signalling*

Received date: 15 February 2020

Revised date: 2 November 2020

Accepted date: 3 November 2020

Please cite this article as: M. de Assis Lima, S.V. da Silva, O. Serrano-Garrido, et al., Metalloprotease ADAMTS-1 decreases cell migration and invasion modulating the spatiotemporal dynamics of Cdc42 activity, *Cellular Signalling* (2020), https://doi.org/10.1016/j.cellsig.2020.109827

Metalloprotease ADAMTS-1 decreases cell migration and invasion modulating the spatiotemporal dynamics of Cdc42 activity

Running title: ADAMTS-1 modulates Cdc42 activity

Maíra de Assis Lima [1†]

E-mail: mlima@usp.br

Suély Vieira da Silva [1†]

E-mail: suelyvieira@usp.br

Orlando Serrano-Garrido [2]

E-mail: orlando.serrano@genyo.es

Maren Hülsemann [3]

E-mail: marenhuelsemann@gmail.com

Luana dos Santos Neres [1]

E-mail: dos.santos.neres_luana@usp.br

Juan Carlos Rodríguez-Manzaneque [2]

E-mail: juancarlos.rodriguez@genyo.es

Louis Hodgson [3]

E-mail: louis.hodgson@einsteinmed.org

Vanessa M Freitas [1*]

E-mail: vfreitas@usp.br

[1] Department of Cell and Developmental Biology, Institute of Biomedical Sciences, University of Sao Paulo, Av. Prof. Lineu Prestes 1524, Ed Biomédicas 1 sala 428, São Paulo, SP 05508-000, Brazil

[2] GENYO. Centre for Genomics and Oncology Research, Avenida de la Ilustración, 114, Granada 18016, Spain.

[3] Department of Anatomy and Structural Biology, Albert Einstein College of Medicine, Bronx, New York, United States of America, Gruss-Lipper Biophotonics Center, Albert Einstein College of Medicine, Bronx, New York, United States of America.

* Corresponding author

[†]These authors contributed equally to this work.

Abstract: ADAMTSs (A Disintegrin And Metalloproteinase with ThromboSpondin motifs) are secreted proteases dependent on Zn^{2+} / Ca^{2+}, involved in physiological and pathological processes and are part of the extracellular matrix (ECM). Here, we investigated if ADAMTS-1 is required for invasion and migration of cells and the possible mechanism involved. In order to test ADAMTS-1's role in ovarian cancer cells (CHO, NIH-OVCAR-3 and ES2) and NIH-3T3 fibroblasts, we modified the levels of ADAMTS-1 and compared those to parental. Cells exposed to ADAMTS-1-enriched medium exhibited a decline in cell migration and invasion when compared to controls with or without a functional metalloproteinase domain. The opposite was observed in cells when ADAMTS-1 was deleted via the CRISPR/Cas9 approach. The decline in ADAMTS-1 levels enhanced the phosphorylated form of Src and FAK. We also evaluated the activities of cellular Rho GTPases from cell lysates using the GLISA® kit. The Cdc42-GTP signal was significantly increased in the CRISPR ADAMTS-1 ES-2 cells. By a Förster resonance energy transfer (FRET) biosensor for Cdc42 activity in ES-2 cells we demonstrated that Cdc42 activity was strongly polarized at the leading edge of migrating cells with ADAMTS-1 deletion, compared to the wild type cells. As conclusion, ADAMTS-1 inhibits proliferation, polarization and migration.

Background

The extracellular matrix (ECM) is composed of a highly organized, three-dimensional structure with many physiological and pathological roles. The ECM, in addition to maintaining tissue integrity, also regulates cell migration, cellular differentiation, proliferation, and provides a reservoir of cytokines and growth factors [1, 2]. This microenvironment consists of tumor-stromal components, fibroblasts, endothelial cells, immune cells, extracellular matrix molecules, growth factors, and proteases that remodel these components. ADAMTS-1 (A Disintegrin And Metalloproteinase with ThromboSpondin type I motifs) was the first described member of the ADAMTS family of metalloproteases and is a well-known extracellular matrix protease [3-6], which can also perform intracellular functions [7, 8]. ADAMTS-1 is secreted proteases dependent on Zn2+ / Ca2+, consisting of six domains which are: pro-domain, metalloproteinase, disintegrin-like, thrombospondin (TSP) homologous domain-containing TSP type I motif, spacer region, and C-terminal TSP motifs [9].

ADAMTS-1 is involved in extracellular matrix processing [10], organogenesis [11], hemostasis functions [12], and it has been identified and expressed during ovulation [13] and in a number of human diseases [14].

In cancer, ADAMTS-1 has an antiangiogenic effect [15, 16], and data from our laboratory show that in triple-negative human breast tumors, tumor tissue presents lower ADAMTS-1 stromal protein levels when compared to the normal tissue [17]. It has been demonstrated that ADAMTS-1 C-terminus is capable of binding to extracellular growth factors including vascular endothelial growth factor (VEGF) [18-20]. ADAMTS-1 sequesters VEGF, preventing this growth factor from binding to its receptor on the cell, leading to impaired migration and cell invasion rates [17]. Our group observed that ADAMTS-1 presence disrupted the signaling induced by Hepatocyte Growth Factor (HGF) in fibrosarcoma cells, reducing migration, proliferation and microtumors formation [21]. However, some studies have shown that ADAMTS-1 has increased expression in tumors with a high degree of malignancy [22], contributing to cancer development [23], including ovarian cancer [24]. In 2006, Liu et al. demonstrated that ADAMTS-1 undergoes auto-proteolytic cleavage and that full-length ADAMTS-1 and the ADAMTS-1 fragments display pro- and anti-tumor activity, respectively. Further investigations have shown that the metalloproteinase activity of ADAMTS-1 was required for its pro-tumor activity, whereas the anti-tumor activity of the ADAMTS-1 fragments required the TSP-1 motif which was likely masked in the full-length molecule [25]. Similar effects on increased angiogenesis were observed with ADAMTS-4 and 13, other members of the ADAMTS family [26, 27].

Here, our goal was to investigate if ADAMTS-1 was involved in regulating migration and invasion in different cell types and the mechanisms used in these processes. We analyzed ovarian cells (CHO, NIH-OVCAR-3 and ES-2) and NIH-3T3 fibroblasts with modified ADAMTS-1 levels and compared those to the wild type cells in order to determine their migration and invasion induces using immunohistochemistry, immunoblot, and migration analyses. We also evaluated the activities of cellular Rho GTPases from cell lysates using the GLISA® kit. The Cdc42-GTP signal was significantly increased in the CRISPR ADAMTS-1 ES-2 cells. We extended on this result using a Förster resonance energy transfer (FRET) biosensor for Cdc42 activity

Our findings point to the critical role of ADAMTS-1 in regulating the dynamics, kinetics and kinematics of protrusions and cell migration, important for invasion in ovarian cancer. Moreover, this protease may modulate and locally control the levels of these processes by binding to extracellular growth factors, thus portending spatiotemporal control of Cdc42 activity during cell migration and invasion.

Results

ADAMTS-1 impacts directional cell migration, independent of its metalloproteinase domain

Ovarian cell lines, CHO, NIH-OVCAR-3, and ES-2, were treated with conditioned medium (C.M.) from HEK 293-T control or HEK 293-T MPA (HEK293T cells overexpressing ADAMTS-1) (Figure 1A). Treatment for 24 hours with the ADAMTS-1-enriched medium did not lead to changes in the cell viability compared to cells treated with the control conditioned medium, measured by MTT assay (Figures 1B – D).

We also observed no difference in cell migration assayed by wound-healing response when comparing CHO or NIH-OVCAR-3 cells treated with C.M. from HEK 293T control with cell treated with C.M. from HEK 293T MPA (Figures 1E and F). Importantly, we found that ES-2 cell migration in the wound-healing assay was significantly impaired in the presence of C.M. from HEK 293T MPA compared to cells treated with HEK 293T control conditioned medium (Figure 1G). These findings indicate that the addition of ADAMTS-1 in the medium affects directional cell migration in cell type dependent manner, and ES-2 cells appear to be highly susceptible to this effect.

To address the cell-type dependent effect of soluble ADAMTS-1 on cell migration, we treated NIH3T3 fibroblasts with C.M. from the wild type HT1080 cells or from the one which overexpressed the full length ADAMTS-1 (ATS1) or ADAMTS-1 with a mutation in the catalytic domain (Z11) (Figure 1H and I). We used the wound-healing assay to evaluate the effect of the soluble ADAMTS-1 on NIH3T3 cells. It was observed that the C.M. enriched in either the full-length ADAMTS-1 or ADAMTS-1 with a mutation in the catalytic domain diminished the directional migration of NIH3T3 cells compared to control conditions treated with the C.M. from the wild type parental HT1080 (Figure 1J and K). These results indicate that soluble ADAMTS-

1 impacts directional cell migration in both ES-2 and fibroblasts and that the catalytic domain function of ADAMTS-1 is not required for the attenuation of migration.

Based on the observed effect of soluble ADAMTS-1 on the ES-2 cell migration, we chose ES-2 as our model cell system and developed a CRISPR/cas9 deletion of ADAMTS-1 in ES-2 cell line (CRISPR ADAMTS-1). The immunofluorescence characterization (Figure 2A), cell lysate, and conditioned medium immunoblot analysis (Figure 2B), all showed a striking decrease in ADAMTS-1 levels in CRISPR ADAMTS-1 compared to the parental ES-2 control cells, without changes in ADAMTS-5 levels. No significant differences in cell proliferation were observed between CRISPR ADAMTS-1 and the wild type ES-2 cells in 5 days and the doubling time in both cells was 24 hours (Figure 2C). Cell migration evaluated using the Transwell assay showed that the CRISPR ADAMTS-1 cells migrated significantly more than the wild type ES-2 cells (Figure 2D and E).

Reduced levels of ADAMTS-1 increase cell invasion and cell proliferation.

The invasive capacity of ADAMTS-1-modulated cells was evaluated by a Matrigel-coated Transwell invasion assay [28]. ES-2 cells treated with C.M. from HEK-293T MPA showed a significant defect in *in vitro* invasion compared to cells treated with the control C.M. (Figure 3A and B). Furthermore, CRISPR ADAMTS-1 cells had a higher invasive capacity compared to the parental ES-2 cells through the Matrigel-coated filters (Figure 3C and D). These results indicate ADAMTS-1 impacts cell invasion through Matrigel, a basement membrane mimicking substrate, pointing to important functional role during cancer invasion.

ADAMTS-1 is able to inhibit endothelial cell proliferation by binding and sequestering growth factors [19, 40-43]. Knowing this, we tested the ability of ES-2 cells to proliferate in response to HGF growth factor (hepatocyte growth factor) in the presence or absence of ADAMTS-1. ES-2 cells are shown to have HGF cognate receptor, c-Met [44]. HGF-treatment increased cell proliferation in CRISPR ADAMTS-1 cells but not in the parental ES-2 cells, as measured using the dye exclusion assay (Figure 3E). This suggests that ADAMTS-1 may impact proliferation capacity of cells in response to a growth factor such as HGF. These results indicate that ADAMTS-1 strongly impacts cell proliferation in response to growth stimulating factors.

The decrease in ADAMTS-1 enhances the phosphorylation of Src and FAK.

To evaluate the status of intracellular signaling components critical for efficient cell motility, we decided to evaluate if ADAMTS-1 may modulate the phosphorylation status of non-receptor tyrosine kinases Src and the focal adhesion kinase (FAK), both are critical for many functions related to cell migration and invasion. When starved cells were stimulated with 1% serum, CRISPR ADAMTS-1 cells significantly elevated the phosphorylation levels of Src-kinase compared to the parental ES-2 control cells (Figure 4A and B). Furthermore, we did not observe changes in the phosphorylation status of FAK (Figure 4A and C) through Western Blotting. Interestingly, we observed an increase both in the number and the area of the punctated immunofluorescence staining patterns of phosphorylated-FAK (Figure 4D, E and F). The measurement of a number of particles and their total area was made using the threshold image (red channel) shown in figure 4F. These observations may point to ADAMTS-1's effects on focal adhesion structure and function due to the observed aggregation of phosphorylated FAK even in absence of the bulk changes in the total levels of phosphorylated FAK, possibly altering the rate of focal adhesion turnover. Next, we compared ES-2 cells treated with HEK 293-T control C.M. to those treated with C.M. from HEK 293-T MPA containing soluble ADAMTS-1, we observed a reduced phosphorylation of Src-kinase ($p = 0.0778$), but no difference in FAK phosphorylation between the groups (Figures Supplementary 1A, B and C). While the total cellular levels of these kinases and their phosphorylation status were not changed, we again observed differences in the number and the area of the punctuated aggregation of phosphorylated FAK in ES-2 cells treated with the control C.M. compared to those treated with C.M. enriched in ADAMTS-1 by immunofluorescence. (Figure Supplementary 1D, E and F). The measurement of the number of particles and their total area was made using the threshold image (red channel) shown in figure supplementary 1F. These results point to alterations in Src and FAK-mediated signaling pathways, dependent on the availability of ADAMTS-1.

Reduced levels of ADAMTS-1 increase and modulate Cdc42 activity.

As we observed the effects of ADAMTS-1 on intracellular signaling components including Src and FAK which affect cell motility and adhesion, we wished to determine what direct regulators of actin cytoskeleton pathways may be altered to lead to this change in the cellular migratory/invasive behaviors. The Rho-family of p21 small GTPases are important signaling molecules that regulate cellular cytoskeleton reorganization and control cell motility [29] . Using

the G-LISA assay, we determined the activity levels of the canonical Rho GTPase Rac1, RhoA and Cdc42 in ES-2 and CRISPR ADAMTS-1 cells. Differences between groups in Rac1 and RhoA analyses were not statistically significant (Supplementary Figure 3). Cdc42 activity levels were decreased in ES-2 cells treated with C.M. from HEK 293T MPA when compared to control (Figure 5A). We observed that the active form of Cdc42 was significantly increased in CRISPR ADAMTS-1 cells compared to the parental ES-2 control cells (Figure 5B). These results indicate the ADAMTS-1 expression modulates the fraction of Cdc42 GTPase that is bound to a guanine triphosphate and in an activated conformation.

Rho GTPases undergo dynamic modulation of activity states during cell migration and motility [30]. As such, G-LISA assays are not able to capture the dynamic modulation of Rho GTPase activity. We turned to Rho GTPase biosensors based on Förster resonance energy transfer (FRET) to monitor the activity modulation of Cdc42 during cell edge protrusions and migration. We produced a set of stable cell lines harboring the previously described FRET-based biosensor for Cdc42 [31] under the tet-OFF inducible promoter in both the parental ES-2 and the CRISPR ADAMTS-1 cell lines. We confirmed the biosensor expression by Western blot analysis showing a single band at approximately 100 kDa which corresponded to the Cdc42 biosensor; this band was not present in non-transduced cells (Figure 5C). First, we imaged Cdc42 biosensor in ES-2 and CRISPR ADAMTS-1 cells and analyzed the Cdc42 activity status by performing the ratiometric image processing, as previously described [32]. We observed that control cells showed lower Cdc42 activity when compared to cells with diminished levels of ADAMTS-1 (Figure 5D). We then measured the dynamics of Cdc42 activity using the live cell imaging modality, under a steady-state condition in which cells were responding to serum in the imaging medium. To quantitatively analyze the live-cell biosensor data, we turned to a previously described Morphodynamics mapping and cross-correlational analysis approach [33]. This technique measures the relative velocities of the edge and correlates these motion parameters to the fluctuation of the GTPase activity at locations along the cell edge where the edge velocities are also measured. We used a computational package [33] that enabled precise edge tracking in time and constructed biosensor measurement windows of the size 0.96 x1.8 µm (3x6 pixels) along the leading edge of the cell. We then tracked and recorded the edge movement during random protrusive events and the associated Cdc42 activity fluctuations both

at the cell edge and at regions successively away from the edge by moving the measurement windows inward in space (Figure 5E) [31]. The Cdc42 activities were then cross-correlated against the edge velocity fluctuations to determine if the two functions were related in time. In figures 5F and G, the times in X-axis are the “Timelag” which indicates the temporal difference between the two functions that are compared by the cross-correlation operation shown. In the case of the parental ES-2 cells, the cross-correlation functions at different spatial positions did not converge in significant, definable peaks, indicating that Cdc42 activity and the edge velocity fluctuations were not correlated and likely decoupled at the signaling pathway level (Figure 5F and H). Interestingly, CRISPR ADAMTS-1 cells show significant positive peaks in the cross-correlation functions at spatial position of 6-9 pixels from the edge that also registers approximately a 20 sec delay from the onset of protrusion initiation (Figure 5G and I). The decoupled versus the coupled Cdc42 activity modulation and the edge motion can be observed in detail by comparing the patterns of oscillations in the morphodynamics maps shown in figures 5H and I. Here, CRISPR ADAMTS-1 cells show more pronounced similarity in morphodynamics maps of both the protrusion velocity (top) and the Cdc42 activity fluctuations (bottom), compared to the ES-2 parental cells. Previous studies in different cell types responding to serum stimulation in medium have shown similar localization of both cross-correlation peak position in space and time for Cdc42 [31, 33, 34]. Our observations point to significant differences in the signaling dynamics in these two cell conditions, suggesting that the signaling pathways are altered in CRISPR ADAMTS-1 cells in such a way that Cdc42 activities are now in delayed synchrony (with ~20 s differential) with the edge motion. This result may suggest the ability of cells to polarize the Cdc42 activation cues more strongly compared to the parental ES-2 cells, and such enhanced signal polarization could lead to an accelerated rate of migration and invasion.

Next, we evaluated the Cdc42 activity in the ES-2 cell line in the presence or absence of ADAMTS-1-enriched medium. We did not observe any difference in whole-cell average levels of Cdc42 activity between ES-2 cells treated with HEK-293T control medium or MPA (Figure Supplementary 2A).Using the cross-correlation analysis, we next determined that there were no significant cross-correlational peaks in Cdc42 activity fluctuation in relation to the cell edge motion in either ES-2 cells treated with conditioned media from the control HEK-293T or with

that overexpressing ADAMTS-1 (Figure Supplementary 2B and D). In figure supplementary 2C and E we plot the maximum cross-correlation coefficient value of each measurement region that was analyzed.

Using the same analysis, we next wished to determine the extent of spatiotemporal coupling of the Cdc42 and the edge velocity during directional cell migration. Cdc42 activity during directional cell migration was measured using the wound-healing assay under live-cell FRET imaging modality. Similar to the random, serum-stimulated protrusion conditions, the basal Cdc42 activation status in the wound-healing assay conditions was more elevated in CRISPR ADAMTS-1 cells compared to the parental ES-2 control cells (Figure 6A). Interestingly, when we observed the cross-correlation function between the protrusion velocity and the Cdc42 activity at the cell edge of control cells in the wound-healing assay, we noted the appearance of significant positive cross-correlation peaks near the edge, in the 3-6, 6-9- and 9-12-pixel regions (Figure 6B). In CRISPR ADAMTS-1 cells, the significant cross-correlation peaks between protrusion movement and Cdc42 activity appear to occurs in narrower regions (3-6 and 6-9 pixels) at the leading edge compared to the control condition (Figure 6D). Interestingly, the spatial position in which the cross-correlation coefficient peak value is the highest has shifted forward in these cells in the presence of directional migratory cues (at 3-6 pixels instead of 6-9 pixels in the control ES-2 cells or in absence of directional migratory cues). These results support the idea that CRISPR ADAMTS-1 cells are able to strongly polarize the dynamics of Cdc42 activity further forward in the protrusive and migratory direction, thus creating a stronger asymmetry in the cell polarity resulting in faster migratory speed and the wound-healing rate. Our results are depicted as a model of signal polarization in figures 6C and E. In control cells, the polarization of Cdc42 activity coordination with the edge motion is more rearward oriented and is more broadly distributed. In contrast, in cells with diminished levels of ADAMTS-1, the highest Cdc42 coordination occurs closer to the leading edge and more sharply focused and polarized, thus enhancing the forward-bias of the cellular signaling asymmetry.

Increasing ADAMTS-1 levels decrease cellular polarity.

Cell polarity depends on the asymmetric organization of cellular components and structures. We evaluated if ADAMTS-1 would be able to alter the cellular polarization of ES-2 cells. We measured the polarization index, defined as the ratio of the cellular length (D) to width (d). We

defined the index values between 1 to 4 as unpolarized or poorly polarized cells. Conversely, index values of greater than 4.1 were considered a fully polarized cell. The parental ES-2 cells showed approximately 60% of cells being fully polarized. Similar results were observed for the CRISPR ADAMTS-1 cells (Figure 6F). Interestingly, when we compared cells treated with the C.M. from control HEK 293-T cells compared to cells treated with the C.M. from HEK 293-T MPA, we observed a strong loss of polarization in cells treated with the C.M. enriched in secreted ADAMTS-1 (Figure 6G). These results indicate that secreted ADAMTS-1 strongly attenuates cellular polarization and could impact the asymmetric distribution of intracellular signaling components and dynamics required for an efficient cell migration and invasion.

Discussion

In this study, we describe that enhanced levels of ADAMTS-1 impacted cell migration and invasion of ovarian cancer cells and fibroblasts. We further show that these effects likely stem from alterations in intracellular signaling topology important for efficient cell motility, including the phospho-regulation of Src-kinase and FAK and the Cdc42 GTPase activation. Our results are in line with previous findings related to the impact of ADAMTS-1 on tumor migration and invasion. It has been shown previously that ADAMTS-1 fragments inhibit lung metastasis of murine mammary carcinoma (TA3) cells and Lewis pulmonary carcinoma cells, and prevent tumor cell proliferation, survival and invasion [25]. Importantly, adverse metastatic and proliferative effects were observed when tumors were exposed to the non-fragmented form of ADAMTS-1 [25], pointing to the mechanism that critically impacts motility and proliferation of tumors. Other ADAMTSs appear to share similar effects, as ADAMTS-4 [26] and ADAMTS-13 [27] have been shown to promote angiogenesis through their metalloproteinase activity. We observed in this work that the metalloproteinase domain is not important for the effect of decreased migration and invasion, corroborating the previous studies by others in this area [25, 27]. The self-proteolysis of full-length enzymes reveals a thrombospondin 1 domain that can interact with VEGF and induce antiangiogenic activity [25-27, 35, 36]. Importantly, our previous works show that ADAMTS-1 disrupts c-Met receptor activation following HGF stimulation by decreasing phosphorylation of tyrosine residue Y1349, which is required for the recruitment of signaling proteins; thus, ADAMTS-1 impaired the activation of ERK 1/2 and FAK signaling pathways related to cell proliferation and motility processes [21]. In contrast to the data shown

in this work, ADAMTS-1 was shown previously to increase migration in a Syndecan-4 expression-dependent manner [37]. The differences here could be that the role and activity of ADAMTS-1 may depend strongly on the presence or the absence of specific extracellular matrix and growth factor conditions.

In vivo, ADAMTS-1 has been shown to inhibit tumor growth when human fibrosarcoma cells, HT-1080, human prostate cancer, DU-145, and Chinese hamster ovary cells, CHO1, are inoculated subcutaneously in mice [38]. GEPIA, a webserver that compares gene expression in human cancer and normal tissues, shows that ADAMTS-1 is more expressed (transcripts per million) in normal ovary tissue (88 donor samples) than on tumor tissues (426 patient samples) http://gepia.cancer-pku.cn/detail.php?gene=ADAMTS1&clicktag=survival [39]. Also, the same webserver shows patients with higher ADAMTS-1 levels presented a superior disease free survival. These data support our findings that ADAMTS-1 presence could interfere with tumor behavior, and decreasing this protease levels would stimulate tumor to growth, migrate and invade. Krampert et al. studied the role of ADAMTS-1 in the healing of skin wounds. In this model, they observed that ADAMTS-1 played different roles in fibroblast migration depending on the concentration; a decrease in the level of this protein stimulated cell migration via the proteolytic activity of ADAMTS-1 [40]. Thus, in our results, the effects of ADAMTS-1 may also be concentration dependent. ADAMTS-1 decreases not only the migratory process of the ES-2 cell line but also decreases its cell division rate, both of which are fundamental processes for tumor development [41]. Although ADAMTS-1 concentration can be controlled by use of approaches including the addition of progesterone [42], more studies of the ADAMTS-1 concentration dependence of cellular functions could be important future areas of investigation.

We also observed the actions of ADAMTS-1 in reducing cell polarity, a fundamental step for the cell migration process. The effects on polarization may be related to changes in the activity of RhoGTPase Cdc42, which showed increased overall activity levels when ADAMTS-1 protease was absent. Not statistically significant however, but we also observed a reduction in the activity of Cdc42 when in the presence of ADAMTS-1-enriched medium, which corroborates this notion. Activation of Cdc42 and cell polarization are important for cell migration and metastasis. In the morphodynamic analysis of CRISPR ADAMTS-1 cells expressing the Cdc42 biosensor we showed that Cdc42 activities are significantly coupled to the edge velocity fluctuation under

random protrusion conditions. This coupling is not observed at all in the parental ES-2 cells under the same condition, pointing to a mechanism in which ADAMTS-1 (or the lack thereof) may regulate the ability of cells to pre-prime the cellular motility machinery for an efficient mobilization upon appropriate presentation of the upstream motility cues. Indeed, in the directional migration model analyzed next, we observed the induction of the coupling of the Cdc42 activity to the edge motion, in the parental ES-2 cells as well as CRISPR ADAMTS-1 cells. Importantly, this induction effect was even more pronounced and exaggerated in the absence of ADAMTS-1 in the CRISPR ADAMTS-1 cells. We observed the forward directional shift in the location of the highest positive cross-correlation between the edge velocity and Cdc42 activity fluctuations in the CRISPR ADAMTS-1 cells, as well as sharpening of the spatial gradient of the correlation coefficient distribution at the cell edge compared to the parental ES-2 cells. These findings indicate for the first time, the role of ADAMTS-1 in directly shaping the intracellular, local-level signaling topology both in space and time, in order to modulate the ability of cells to migrate and invade more efficiently. Our observations from the CRISPR ADAMTS-1 cells were corroborated by the data from the C.M. treatment of ES-2 cells (control or ADAMTS-1 enriched). Here, ADAMTS-1-enriched C.M. treatment appeared to strongly suppress the coupling of Cdc42 activity to edge movement, pointing to changes in signaling pathways that could otherwise lead to Cdc42-dependent mechanisms. These results point to a role of ADAMTS-1 protease that impacts Cdc42 regulation on ES-2 cell polarity and the control of cell motility machinery.

The molecular pathways resulting in alterations of the Cdc42 activity dynamics during ADAMTS-1 modulation in our cell lines is beyond the scope of the current study. However, others have shown that the relationship between extracellular interaction and potential sequestration of important growth factors cells respond to by ADAMTS-1, may alter the signaling topology and dynamics targeting Cdc42 activation. Importantly, previous studies have shown that the carboxy-terminal domain of ADAMTS-1 was found to be responsible for a growth factor VEGF sequestration [20]. This ADAMTS-1 sequestration of VEGF likely inhibits several VEGF functions, including its role in cell migration and invasion, not only in endothelial cells [20]. In MDA-MB-231 human breast adenocarcinoma cells, the neuropillin1 signal (NRP1) produced by the long VEGF isoform reduces the expression of ARHGAP17 and activates Cdc42; thus,

increased activation of Cdc42 in these cells may consequently increase cell migration [43]. In addition, ADAMTS-1 has been shown to regulate syndecan-4 expression on the cell surface, and in endothelial cells both molecules act via VEGF sequestration and inhibition of angiogenesis. ADAMTS-1 influences syndecan-4 levels on the cell surface by regulating MMP-9 production leading to ECM regulation, inhibition of migration, and modulation of integrin adhesions [16]. Together, these previous observations and our new findings point to how ADAMTS-1 may regulate the cellular motility microenvironment, by modulating both the extracellular availability and function of the pertinent growth factors, as well as consequently impacting signaling pathways regulating the cytoskeleton reorganization including the Rho family GTPases activation dynamics. Pathways that may be altered to produce these phenotypes include signaling proteins related to the control of focal adhesion dynamics, as well as those regulating the balance of activities between Cdc42 and others Rho family GTPases, including Rac1 and RhoA. The coordination of Rho GTPases is exquisitely controlled by the balance of Rho GEFs, GAPs, and GDIs activities. These regulators, in turn, are controlled and organized spatially and temporally through interacting with kinases, signaling complexes, and cytoskeleton proteins. Thus, the altered signaling scenario propagated by changes in ADAMTS-1 expression levels and functions in the context of cell migration may impact these Rho regulators to alter the spatiotemporal organization of the activation topology in protrusion and migration, ultimately regulating tumor invasion and metastasis.

Methods

Cell lines and cell culture conditions

ES-2, CHO, and NIH-OVCAR-3 cells (ATCC) were cultured in Dulbecco's modified Eagle medium /Ham's F-12 medium (DMEM/F12) (Sigma Aldrich) and HT1080 cells (wild type, overexpressing ADAMTS-1 full length or overexpressing ADAMTS-1 with a mutation in the catalytic domain) were developed as previously described [11] and NIH-3T3 were cultured in DMEM (Sigma Aldrich), both supplemented with 10% FBS and penicillin/streptomycin (100 I.U./mL and 100 µg/mL, respectively) under a humidified atmosphere of 5% CO_2 at 37°C.

Treatment of cell lines with conditioned medium from HT1080 or HEK293T cells overexpressing ADAMTS-1

The overexpressing HT1080 ADAMTS-1 full length (ATS1) or ADAMTS-1 with a mutation in the catalytic domain (Z11) were established as described previously. The mutation consisted in the single substitution of residue E385 to A at the zinc-binding site to disable the catalytic activity of ADAMTS1 [11]. HEK293T cells overexpressing ADAMTS-1 were established as described previously and termed HEK293T-MPA-mcherry/puromycin/ADAMTS-1 [21]. Shaw et al. 2002 [44] performed a HEK293 microarray analysis and no transcript of any member of ADAMTS's family was detected. The increase in ADAMTS-1 levels in the transduced cells was verified by Western blotting. HEK293T cells were plated on 100 mm cell culture plates and when reached 90% of confluence, 10 mL of DMEM / Ham's F-12 medium without SFB was added and conditioned for 24 hours, the collected medium was centrifuged and filtered in a syringe with 0.45 membrane filter to remove cell debris. The obtained medium was pooled, aliquoted and then frozen at -80 ° C. The same conditioned medium was used in all the experiments that were carried out. The ovarian cell lines were treated with either the ADAMTS-1 enriched media (MPA) or the conditioned medium from the control HEK293T cells without ADAMTS-1 overexpression (MPC).

Viability by Trypan Blue dye exclusion analysis

Trypan blue (Sigma Chemical Co., St. Louis, MO, USA) was used to determine the number of viable cells present in the cell suspension. Each 10 µl of the cell suspension was mixed to 10 µl Trypan blue. Then the cells were examined by the Countess ™ II Automated Cell Counter equipment (Thermo Fischer, Waltham, Massachusetts, USA) to determine if the cells absorbed or deleted the dye. Cells that absorbed the dye were defined as non-viable; those that excluded were considered viable.

MTT assay

MTT (3-(4,5-Dimethylthiazol-2-yl)-2,5-Diphenyltetrazolium Bromide) is used to assess cell viability as a function of redox potential. Actively respiring cells convert the water-soluble MTT to an insoluble purple formazan. The formazan is then solubilized and its concentration determined by optical density. The cell culture supernatant was first removed, and 100 µL of fresh DMEM /F-12 and 10 µL MTT medium (Calbiochem, Darmstadt, Germany) was added at 5 mg / mL in 1x PBS to a final concentration. 0.5 mg / mL. The cells were kept in the incubator for 3 hours at 37 ° C in an atmosphere containing 5% CO_2 until the formation of blue crystals.

100µL DMSO was then added to dissolve the crystals, the wells were homogenized, and the absorbance at 540 nm was measured using a spectrophotometer (Epoch Microplate Spectrophotometer, BioTek, Winooski, VT, USA).

Wound-healing assay

The cells were grown in 60 mm^2 plates until they reached the confluence of 80%. An "wound" was made in the monolayer by gently passing a 10 µL pipette tip over it. This passage produced a discontinuity in the cell monolayer, whose cells on its margin tended to migrate into the empty spaces. Reference points were demarcated at the bottom of each plate to allow photomicrographs with the Canon PowerShot G6 (Canon, Tokyo, Japan) to be obtained from the same “wound” region at different times (0 and 24 hours). Cell migration was evaluated by quantifying the remaining cell-free area within the wound channel (arbitrarily marked as a cell-free region) and was measured by using the ImageJ program (https://gdc-portal.nci.nih.gov/). The percentage decline of the “wound” area was characterized to determine the cell migration index.

CRISPR/Cas9

The commercially obtained PX330 (U6-Chimeric_BB-CBh-hSpCas9) expression vector (Catlog # 42230 - Addgene, Watertown, MA, USA) was digested with restriction enzyme Bbs1 (ER1011, Thermo Fischer, Waltham, Massachusetts, USA) and ligated together with the oligonucleotide encoding the guide RNA designed against ADAMTS-1 to produce a missense mutation (using http://crispr.mit.edu/) according to the protocol of Zhang Lab [45]. The plasmid containing the guide RNA oligonucleotide was transfected into cells using lipofectamine 2000 following the manufacturer’s protocols (Thermo Fischer, Waltham, Massachusetts, USA). 72 hours following transfection, cells were selected with Puromycin (Thermo) at a concentration of 4 µg/mL for 4 days.

Immunofluorescence and Phalloidin staining

Cells grown on glass coverslips were fixed in 4% paraformaldehyde in phosphate-buffered saline (PBS) for 10 min, rinsed and permeabilized with 0.5 % Triton X-100 (Sigma) in PBS for 10 min. Fixed and permeabilized cells were rinsed and blocked with Normal Goat Serum (10 %) for 1 h, followed by incubation with primary antibody rabbit polyclonal against ADAMTS-1 (1:200

- MAB1810, Millipore). Cells were then incubated with Alexa 568-secondary antibody and Phalloidin-Alexa Fluor 488 (Invitrogen). Samples were mounted in ProLong antifade reagent with DAPI (Invitrogen). Samples were analyzed using a widefield fluorescence microscope equipped with a 63x PlanApo 1.3 NA objective (Axiophot, Carl Zeiss, Oberkochen, Germany), equipped with a digital CCD camera (CoolSnap HQ2, Photometrics Inc, Tucson, AZ, USA). To evaluate phosphorylation of FAK and Src staining, red channel was analyzed; a threshold area was determined and then measured using ImageJ public domain software (http://rsb.info.nih.gov/ij/).

Western blot

Cells were lysed in RIPA buffer (150 mM NaCl, 1.0% NP-40, 0.5% deoxycholate, 0.1% SDS, 50 mM Tris pH 8.0) containing a protease inhibitor cocktail and phosphatase inhibitor (Sigma). After centrifugation (10,000 g) for 10 min at 4 °C, the supernatants were recovered and quantified (Bradford reagent, Bio-Rad). For SDS-PAGE, 30 µg of protein from lysate were loaded per well and separated in 10% polyacrylamide gel (prepared with 1.5M Tris-HCl, 10% SDS, 30% bis-acrylamide, 10% ammonium persulfate, and TEMED). Gel proteins were transferred to a Hybond ECL nitrocellulose membrane (Amersham); the membrane was blocked with TBS containing 5% non-fat milk for 1 hour at 4 °C. After a wash in TBS with 0.05% Tween 20 (TBST), the membrane was probed with antibodies against polyclonal anti-Cdc42 (P1), Santa Cruz and monoclonal anti-β-actin (AC15), Santa Cruz. A fluorescent secondary antibody was used to detect proteins on the membrane. The membranes also were probed with antibodies against ADAMTS-1 (1:2000 - MAB1810, Millipore), ADAMTS-5 (1:1000-ab41037, Abcam), cSrc (1:1000 – 36D10, Cell Signaling), p-cSrc (1:1000 – D49G4, Cell Signaling), FAK (1:1000 – SC932, Santa Cruz) and p-FAK (1:1000 – SC1656R, Santa Cruz) and β-actina (1:4000 - A2228, Sigma). In these cases, bands were detected by peroxidase-conjugated secondary antibodies and developed with chemiluminescence reagent (Bio-rad, Hercules, California, EUA). The membranes were stripped with the Restore Western Blot Stripping Buffer (Pierce, Thermo Fischer, Waltham, Massachusetts, USA) and re-probed as required.

Growth curve

The cells were plated on 35 mm plates at a density of 5 x 10^4 cells per plate and maintained in DMEM / Ham's F12 medium with 10% FBS at 37 °C in an atmosphere containing 5% CO_2. The total number of live and dead cells was counted every day for a total of 3 days. For cell counting, cells were lifted and suspended in DMEM / Ham's F12 medium and the Countess ™ II Automated Cell Counter apparatus (Thermo Fischer, Waltham, Massachusetts, USA) was used, following the manufacturer's protocols.

Proliferation Assay

The cells were serum starved for 24 hours, and plated on 60 mm plates at a density of 1 x 10^4 cells per plate and maintained in DMEM / Ham's F12 medium with 10% FBS at 37 °C in an atmosphere containing 5% CO_2. ES-2 wild-type cells or those with the deleted ADAMTS-1 gene (CRISPR ADAMTS-1) were maintained in the absence or presence of 10% SFB for 24h, or in the absence or presence of 10 ng/ml HGF for 24 hours. After this period the cells were stained with trypan blue and the number of live and dead cells were counted in each sample as described above.

Migration and invasion assays

Polycarbonate membranes with 8 µm pores in 10-well Boyden chambers (Neuro Probe ®) were used for the migration and invasion assays. In migration assays, cells with modified levels of ADAMTS-1 and control cells (1 x 10^5) were plated into the upper chamber containing 800 µL of DMEM / F12 medium without serum. The lower chamber was filled with 800 µL of DMEM / F12 with 5% serum and incubated under standard cell culture conditions for 24 hrs. Following the incubation, the membrane with the cells was fixed with 4% paraformaldehyde and post-fixed with 0.2% crystal violet in 20% methanol. Cells on the upper side of the filter were removed with a cotton swab. The migrated cells on the lower side of the filter were photographed and counted. For the invasion assays, the filters were coated with10 µl of Matrigel (Trevigen Inc, Gaithesburg, MD, USA, 10-13 mg/ml). Cells (1 x 10^5) were plated into the upper chamber containing 800 µL of DMEM / F12 without serum. The lower chamber was filled with 800 µL of DMEM / F12 ADAMTS-1. After 48 hours in culture, the cells were fixed and stained. Cells on the filter upper side were removed, whereas the invading cells on the filter lower side were stained, photographed and counted.

Detection of activated Cdc42 / RhoA / Rac1 using G-LISA

Cdc42 / RhoA / Rac1 G-LISA kit (Cytoskeleton, Inc., Denver, CO, USA) was used to quantify the levels of GTP-loaded, activated Rho GTPases, following the manufacturer's protocols. The degree of activation of Cdc42 / RhoA / Rac1 was determined by the absorbance measured at 490 nm wavelength using an Epoch Microplate Spectrophotometer (BioTek, Winooski, VT, USA). For the negative controls, Cdc42 / RhoA / Rac1 activity levels were measured from cell lysates obtained from serum-deprived cells.

Generation of Stable ES-2 cell line with Inducible Expression of Rho GTPase Biosensors

A Two-step, retroviral transduction protocol was used to produce a stable and biosensor inducible ES-2 cell line, following previously established protocols [46]. Briefly, the stable incorporation of tet-OFF transactivator (tTA) was achieved using the G418 selection (1 mg/mL) as previously described [46]. For the integration of inducible Cdc42-biosensor cassette, we infected the stable tet-OFF cells successively by monitoring the level of biosensor fluorescence as a function of the number of viral transductions performed, followed by selection using Zeocin (1 mg/mL). In order to repress the biosensor expression in normal cell culture conditions, the cell culture medium was supplemented with 1 µg/mL Doxycyclin (Dox). To induce Cdc42 biosensor expression, Dox was removed 48 hrs prior to imaging by detaching cells through brief trypsinization and then replating at 1×10^4 cells per 10 cm dish. Biosensor-induced cells were then plated on glass coverslips for 2 hrs prior to imaging.

Microscopy imaging and analysis for Cdc42 biosensor inducible cells

The Cdc42 activities were measured by imaging the ratio of the biosensor FRET emission to the donor mCerulean emission upon donor excitation. For live cell experiments using ES-2 cells, images were acquired at 40× magnification (Olympus UIS2 40× N/A 1.3) using a custom microscope capable of simultaneous acquisitions of FRET with mCerulean emission channels, through two CoolsnapES2 (Photometrics) cameras mounted via a beamsplitter [28]. Images simultaneously acquired were aligned correctly for a pixel-by-pixel matching using *a priori* calibration and coordinate transformation-based morphing to achieve accurate registration prior to ratiometric calculations, as described previously [32]. Image processing, including the pixel read noise subtraction, flat-field correction, background subtraction, ratio calculations, and

correction for photobleaching, were performed as described previously [32]. For fixed cell imaging of ES-2, a single CoolsnapHQ2 (Photometrics) camera attached on the bottom port of the microscope was used. In this case, excitation and emission filter wheels allowed for the switching of appropriate filter sets to acquire mCerulean and the FRET emission acquisitions. The optical specifications for this configuration of the system used are detailed elsewhere [28]. In both live-cell imaging and fixed-cell imaging, transilluminated images were also obtained. For imaging of fixed cells overexpressing the biosensor, we controlled for the relative expression levels by imaging only those cells that had brightness to fill approximately 80% of the 12-bit digitization range of the CCD chip, using excitation intensities of approximately 0.4–1.0 mW at the specimen plane.

Morphodynamics analysis and cross-correlation studies

Morphodynamics analysis approach was described previously [33]. Briefly, the algorithm tracks the leading-edge motion by using a previously described method [33, 47]. The measurement window segments are then defined along the cell edge in order to measure the parameters of interest within single, independent window segment entities. The window segments of size 3 x 6 pixels (308 nm/pixel at the specimen plane) were constructed along the leading edge of cells and tracked along the cell edge motion during complete protrusion-retraction cycles. We have previously determined that this particular measurement window dimension was diffusion-limited within the conditions of imaging (10 s interval time lapse), the 40x objective magnification, and the pixel dimension of the imaging system used [33]. This ensures that each window segment can be considered an independent measurement entity in our calculations [33] and achieve sufficient statistical power, as in our previous studies [33, 34, 48-50]. The window segments were also moved away from the leading edge in 3 pixel increments to measure biosensor activities at distal regions from the leading edge. The coupling between changes in the Cdc42 biosensor activity and the motion of the cell edge was determined using cross-correlation function *xcov* in Matlab; Pearson's correlation coefficient was used to determine the strength of cross-correlation between the activity fluctuation and the motion of the cell edge. In this work, n= 120 window segments from 14 cells for the parental ES-2 cells, n= 120 window segments from 14 cells for CRISPR ADAMTS-1 ES-2 cells, both undergoing random protrusions in response to serum, and n=180 window segments from 10 cells for the parental ES2 cells,

n=180 window segments from 12 cells for CRISPR ADAMTS-1 ES-2 cells, both undergoing wound-healing motility response, were measured and characterized. The cell data analyzed were each pooled from 5-6 independent experiments. The numbers of individual window segments constructed and total number of cells analyzed per cell populations/conditions were similar to previous studies [33, 34, 48-50]. The cross-correlation functions between the edge motion and the corresponding fluctuations in Cdc42 activities were analyzed using the 2000x bootstrapping of the smooth-spline-fit functions from the per-cell averages of the individual window segments to determine the 95% confidence intervals. The autocorrelation function of the edge protrusion velocities was used to indicate the characteristic periodicity of the intrinsic protrusion-retraction cycles, as in previous studies [33, 34, 48-50]. The morphodynamic analysis as used herein and in our previous studies [33, 34, 48-50], does not separately account for the behavior of protein activities as a function of either protrusion or retraction. Instead, a global cross-correlation function is produced, taking into account many cycles of these processes. By imaging the steady-state behavior, we are able to sample many iterations of protrusion-retraction behaviors and build statistically robust cross-correlation function between the two signaling nodes.

Cell polarization

For cell polarization analysis the cells were plated in 6-well plates (Corning, New York, USA) for 24 hrs, then serum-starved for an additional 24 hrs. The wild type or CRISPR ADAMTS-1 cells were then treated with DMEM / Ham's F12 medium (Sigma Chemical Co, St Louis, MO, USA) supplemented with 1% serum (Gibco) for 24 hrs. ES-2 cells were also treated with the conditioned medium from HEK 293T control or overexpressing ADAMTS-1 supplemented with 1% serum for 24 hours. Following these treatments, images were taken using a Canon PowerShot G6 camera (Canon, Tokyo, Japan). An average of 160 cells per group was analyzed using ImageJ software (https://gdc-portal.nci.nih.gov/), in which we measured the cell length (D) and width (d), and produced a ratio of D / d, describing the cell polarization.

Statistical analysis

Student's t-test was performed to evaluate differences between the two groups. Differences between three or more groups were assessed by analysis of variance (ANOVA), followed by

Bonferroni's multiple comparisons test. The software used was GraphPad Prism (GraphPad Software, Inc., San Diego, CA).

Acknowledgements

The authors want to thank CNPq and FAPESP.

Funding

This investigation was supported by The State of São Paulo Research Foundation (FAPESP grants 2015/19773-5, 2018/19813-5 and 2018/05566-6), and the Brazilian National Council for Scientific and Technological Development (CNPq grant 142302/2015-5). National Institutes of Health grant R35GM136226 to L.H. L.H. is an Irma T. Hirschl Career Scientist. Grant from Ministerio de Economía y Competitividad and Instituto de Salud Carlos III from Spain, co-financed by FEDER (PI16/00345 to JCRM)".

Authors' contributions

MAL and VMF designed this study. MAL and SVS performed the experiments and analyzed the data and wrote the original manuscript draft. LH developed the Cdc42 biosensor. LH and MH helped in the development and analyses of the ES-2 cell line expressing Cdc42 biosensor using the tet-off system. LSN performed experiments for the revised manuscript. JCRM developed the HT1080 cells with ADAMTS-1 metalloproteinase domain mutation. JCRM and OSG helped with the analyses of the data. MAL and VMF prepared the manuscript. All authors reviewed and approved the manuscript. VMF and LH contributed to discussions and interpretations of the results; reviewed, edited, and approved the final manuscript.

References

[1] P. Zigrino, S. Löffek, C. Mauch, Tumor-stroma interactions: their role in the control of tumor cell invasion, Biochimie 87(3-4) (2005) 321-8.
[2] A.D. Theocharis, S.S. Skandalis, C. Gialeli, N.K. Karamanos, Extracellular matrix structure, Adv Drug Deliv Rev 97 (2016) 4-27.

[3] K. Kuno, Y. Okada, H. Kawashima, H. Nakamura, M. Miyasaka, H. Ohno, K. Matsushima, ADAMTS-1 cleaves a cartilage proteoglycan, aggrecan, FEBS Lett 478(3) (2000) 241-5.
[4] S. Porter, I.M. Clark, L. Kevorkian, D.R. Edwards, The ADAMTS metalloproteinases, Biochem J 386(Pt 1) (2005) 15-27.
[5] L. Wagstaff, R. Kelwick, J. Decock, D.R. Edwards, The roles of ADAMTS metalloproteinases in tumorigenesis and metastasis, Front Biosci (Landmark Ed) 16 (2011) 1861-72.
[6] R. Kelwick, I. Desanlis, G.N. Wheeler, D.R. Edwards, The ADAMTS (A Disintegrin and Metalloproteinase with Thrombospondin motifs) family, Genome Biol 16 (2015) 113.
[7] S.V. Silva, M.A. Lima, N. Cella, R.G. Jaeger, V.M. Freitas, ADAMTS-1 Is Found in the Nuclei of Normal and Tumoral Breast Cells, PLoS One 11(10) (2016) e0165061.
[8] K. Kuno, H. Iizasa, S. Ohno, K. Matsushima, The exon/intron organization and chromosomal mapping of the mouse ADAMTS-1 gene encoding an ADAM family protein with TSP motifs, Genomics 46(3) (1997) 466-71.
[9] K. Kuno, K. Bannai, M. Hakozaki, K. Matsushima, K. Hirose, The carboxyl-terminal half region of ADAMTS-1 suppresses both tumorigenicity and experimental tumor metastatic potential, Biochem Biophys Res Commun 319(4) (2004) 1327-33.
[10] H. Stanton, J. Melrose, C.B. Little, A.J. Fosang, Proteoglycan degradation by the ADAMTS family of proteinases, Biochim Biophys Acta 1812(12) (2011) 1616-29.
[11] J.C. Rodríguez-Manzaneque, J. Westling, S.N. Thai, A. Luque, V. Knauper, G. Murphy, J.D. Sandy, M.L. Iruela-Arispe, ADAMTS1 cleaves aggrecan at multiple sites and is differentially inhibited by metalloproteinase inhibitors, Biochem Biophys Res Commun 293(1) (2002) 501-8.
[12] R.C. Salter, T.G. Ashlin, A.P. Kwan, D.P. Ramji, ADAMTS proteases: key roles in atherosclerosis?, J Mol Med (Berl) 88(12) (2010) 1203-11.
[13] D.L. Russell, H.M. Brown, K.K. Dunning, ADAMTS proteases in fertility, Matrix Biol 44-46 (2015) 54-63.
[14] T.J. Mead, S.S. Apte, ADAMTS proteins in human disorders, Matrix Biology (2018) 71-72:225-239.
[15] F. Vázquez, G. Hastings, M.A. Ortega, T.F. Lane, S. Oikemus, M. Lombardo, M.L. Iruela-Arispe, METH-1, a human ortholog of ADAMTS-1, and METH-2 are members of a new family of proteins with angio-inhibitory activity, J Biol Chem 274(33) (1999) 23349-57.
[16] J. Lambert , K. Makin , S. Akbareian , R. Johnson , S.D. Robinson, D.R. Edwards, ADAMTS - 1 and Syndecan - 4 intersect in the regulation of cell migration and angiogenesis, bioRxiv (2019).
[17] V.M. Freitas, J.B. do Amaral, T.A. Silva, E.S. Santos, F.R. Mangone, J.e.J. Pinheiro, R.G. Jaeger, M.A. Nagai, G.M. Machado-Santelli, Decreased expression of ADAMTS-1 in human breast tumors stimulates migration and invasion, Mol Cancer 12 (2013) 2.
[18] K. Bourd-Boittin, D. Bonnier, A. Leyme, B. Mari, P. Tuffery, M. Samson, F. Ezan, G. Baffet, N. Theret, Protease profiling of liver fibrosis reveals the ADAM metallopeptidase with thrombospondin type 1 motif, 1 as a central activator of transforming growth factor beta, Hepatology 54(6) (2011) 2173-84.
[19] M.L. Iruela-Arispe, D. Carpizo, A. Luque, ADAMTS1: a matrix metalloprotease with angioinhibitory properties, Ann N Y Acad Sci 995 (2003) 183-90.

[20] A. Luque, D.R. Carpizo, M.L. Iruela-Arispe, ADAMTS1/METH1 inhibits endothelial cell proliferation by direct binding and sequestration of VEGF165, J Biol Chem 278(26) (2003) 23656-65.
[21] H. Noriega-Guerra, M.C. Cruz, P.R.L. Ribeiro, J. Strnadel, H. Wang, R.L. Klemke, R.G. Jaeger, V.M. Freitas, ADAMTS-1 disrupts HGF/c-MET signaling and HGF-stimulated cellular processes in fibrosarcoma, Exp Cell Res 363(2) (2018) 271-282.
[22] T. Masui, R. Hosotani, S. Tsuji, Y. Miyamoto, S. Yasuda, J. Ida, S. Nakajima, M. Kawaguchi, H. Kobayashi, M. Koizumi, E. Toyoda, S. Tulachan, S. Arii, R. Doi, M. Imamura, Expression of METH-1 and METH-2 in pancreatic cancer, Clin Cancer Res 7(11) (2001) 3437-43.
[23] *Y. Mohamedi*, *T. Fontanil*, *T. Cobo*, *J.A. Vega*, *J.L. Cobo*, *O. García-Suárez*, *J. Cobo*, *S. Cal*, *Á. J. Obaya*, The molecular interaction of ADAMTS-1 and fibulin-1 and its potential contribution to breast cancer biology, Journal of Cancer Metastasis and Treatment, 2019, p. 5:37.
[24] M.A. Lima, L.d. Santos, A. Turric, S. Nonogaki, M. Buim, J.H. Lima, C.A.B.d.T. Osório, F. Soares, V.M. Freitas, Levels of ADAMTS proteases and their substrates in epithelialovarian tumors with different behavior, Pathobiology (2016).
[25] Y.J. Liu, Y. Xu, Q. Yu, Full-length ADAMTS-1 and the ADAMTS-1 fragments display pro- and antimetastatic activity, respectively, Oncogene 25(17) (2006) 2452-67.
[26] N. Rao, Z. Ke, H. Liu, C.J. Ho, S. Kumar, W. Xiang, Y. Zhu, R. Ge, ADAMTS4 and its proteolytic fragments differentially affect melanoma growth and angiogenesis in mice, Int J Cancer 133(2) (2013) 294-306.
[27] M. Lee, E.S. Rodansky, J.K. Smith, G.M. Rodgers, ADAMTS13 promotes angiogenesis and modulates VEGF-induced angiogenesis, Microvasc Res 84(2) (2012) 109-15.
[28] A. Albini, Y. Iwamoto, H.K. Kleinman, G.R. Martin, S.A. Aaronson, J.M. Kozlowski, R.N. McEwan, A rapid in vitro assay for quantitating the invasive potential of tumor cells, Cancer Res 47(12) (1987) 3239-45.
[29] A.A. Schmitz, E.E. Govek, B. Bottner, L. Van Aelst, Rho GTPases: signaling, migration, and invasion, Exp Cell Res 261(1) (2000) 1-12.
[30] D. Spiering, L. Hodgson, Dynamics of the Rho-family small GTPases in actin regulation and motility, Cell Adh Migr 5(2) (2011) 170-80.
[31] S. Hanna, V. Miskolci, D. Cox, L. Hodgson, A New Genetically Encoded Single-Chain Biosensor for Cdc42 Based on FRET, Useful for Live-Cell Imaging, PLoS One 9(5) (2014) e96469.
[32] D. Spiering, J.J. Bravo-Cordero, Y. Moshfegh, V. Miskolci, L. Hodgson, Quantitative Ratiometric Imaging of FRET-Biosensors in Living Cells, Methods in cell biology 114 (2013) 593-609.
[33] M. Machacek, L. Hodgson, C. Welch, H. Elliott, O. Pertz, P. Nalbant, A. Abell, G.L. Johnson, K.M. Hahn, G. Danuser, Coordination of Rho GTPase activities during cell protrusion, Nature 461(7260) (2009) 99-103.
[34] L. Hodgson, D. Spiering, M. Sabouri-Ghomi, O. Dagliyan, C. DerMardirossian, G. Danuser, K.M. Hahn, FRET binding antenna reports spatiotemporal dynamics of GDI-Cdc42 GTPase interactions, Nat Chem Biol 12(10) (2016) 802-9.
[35] J. Dubail, F. Kesteloot, C. Deroanne, P. Motte, V. Lambert, J.M. Rakic, C. Lapière, B. Nusgens, A. Colige, ADAMTS-2 functions as anti-angiogenic and anti-tumoral molecule independently of its catalytic activity, Cell Mol Life Sci 67(24) (2010) 4213-32.

[36] B. Renganathan, V. Durairaj, D.C. Kirman, P.K.A. Esubonteng, S.K. Ang, R. Ge, Recombinant TSR1 of ADAMTS5 Suppresses Melanoma Growth in Mice via an Anti-angiogenic Mechanism, Cancers (Basel) 10(6) (2018).
[37] J.C. Rodríguez-Manzaneque, D. Carpizo, M.e.C. Plaza-Calonge, A.X. Torres-Collado, S.N. Thai, M. Simons, A. Horowitz, M.L. Iruela-Arispe, Cleavage of syndecan-4 by ADAMTS1 provokes defects in adhesion, Int J Biochem Cell Biol 41(4) (2009) 800-10.
[38] M. Obika, H. Ogawa, K. Takahashi, J. Li, O.F. Hatipoglu, M.Z. Cilek, T. Miyoshi, J. Inagaki, T. Ohtsuki, S. Kusachi, Y. Ninomiya, S. Hirohata, Tumor growth inhibitory effect of ADAMTS1 is accompanied by the inhibition of tumor angiogenesis, Cancer Sci 103(10) (2012) 1889-97.
[39] Z. Tang, C. Li, B. Kang, G. Gao, C. Li, Z. Zhang, GEPIA: a web server for cancer and normal gene expression profiling and interactive analyses, Nucleic Acids Res 45(W1) (2017) W98-W102.
[40] M. Krampert, S. Kuenzle, S.N. Thai, N. Lee, M.L. Iruela-Arispe, S. Werner, ADAMTS1 proteinase is up-regulated in wounded skin and regulates migration of fibroblasts and endothelial cells, J Biol Chem 280(25) (2005) 23844-52.
[41] D. Hanahan, R.A. Weinberg, Hallmarks of cancer: the next generation, Cell 144(5) (2011) 646-74.
[42] M.A. Lima, S.V. da Silva, V.M. Freitas, Progesterone acts via the progesterone receptor to induce adamts proteases in ovarian cancer cells, J Ovarian Res 9(1) (2016) 9.
[43] M. Kiso, S. Tanaka, S. Saji, M. Toi, F. Sato, Long isoform of VEGF stimulates cell migration of breast cancer by filopodia formation via NRP1/ARHGAP17/Cdc42 regulatory network, Int J Cancer 143(11) (2018) 2905-2918.
[44] G. Shaw, S. Morse, M. Ararat, F.L. Graham, Preferential transformation of human neuronal cells by human adenoviruses and the origin of HEK 293 cells, FASEB J 16(8) (2002) 869-71.
[45] L. Cong, F. Zhang, Genome engineering using CRISPR-Cas9 system, Methods Mol Biol 1239 (2015) 197-217.
[46] V. Miskolci, L. Hodgson, D. Cox, Using Fluorescence Resonance Energy Transfer-Based Biosensors to Probe Rho GTPase Activation During Phagocytosis, Methods Mol Biol 1519 (2017) 125-143.
[47] M. Machacek, G. Danuser, Morphodynamic Profiling of Protrusion Phenotypes, Biophys. J. 90(4) (2006) 1439-1452.
[48] D.M. Shcherbakova, N. Cox Cammer, T.M. Huisman, V.V. Verkhusha, L. Hodgson, Direct multiplex imaging and optogenetics of Rho GTPases enabled by near-infrared FRET, Nat Chem Biol (2018).
[49] V. Miskolci, B. Wu, Y. Moshfegh, D. Cox, L. Hodgson, Optical Tools To Study the Isoform-Specific Roles of Small GTPases in Immune Cells, J Immunol 196(8) (2016) 3479-93.
[50] J. Zawistowski, M. Sabouri-Ghomi, G. Danuser, K. Hahn, L. Hodgson, A RhoC biosensor reveals differences in the activation kinetics of RhoA and RhoC in migrating cells, Plos One In Press (2013).

Figure Captions

Figure 1 Treatment of the cell line ES-2 with C. M. from HEK 293-T MPA decreases cell migration compared to control without affecting cell viability with or without the

metalloproteinase domain. Western blots of ADAMTS-1 expression in HEK 293-T cells transduced with the pReceiver-Lv213 lentiviral vector (MPA) relative to non-transduced cells (control) (A). Verification of cell viability of ovarian cell lines CHO (B), NIH-OVCAR-3 (C) and ES-2 (D) treated with C.M. from HEK 293-T MPA or the control, by MTT assay. Measurement of cell migration by the wound-healing assay of cell lines CHO (E), NIH-OVCAR-3 (F) and ES-2 (G) treated with C.M. from HEK 293-T MPA or control. Western Blotting showing the overexpression of ADAMTS-1 full length (ATS1) and mutated in metalloproteinase domain (Z11) in HT1080 cell compared to wild type cells, in cell lysates (H) and in the Conditioned medium (I). Quantification of the wound-healing assay using NIH3T3 fibroblasts, treated with the C.M. from HT1080 cells, either wild type, ATS1 or Z11 overexpressors (J). D, Representative images of the wound-healing assays, from (K). N=3 independent experiments; Student-t test (two-tail), * $p < 0.05$. Error limits are +/- SEM.

Figure 2 Deletion of ADAMTS-1 increases the migration of ES-2 cells. ADAMTS-1 levels in the ES-2 cells were reduced following the CRISPR / Cas9-mediated gene deletion, shown either by immunofluorescence (A) or by Western Blotting. Reduction of ADAMTS-1 is observed both in the lysate and the conditioned medium, ADAMTS-5 in the cell lysate is not altered (B). ES-2 CRISPR ADAMTS-1 cells present proliferation rate similar to the ES-2 Wild Type (C). Genetic deletion of ADAMTS-1 results in increased cell migration of ES-2 cells in an *in vitro* transwell assay (D). E, Representative fields of view are shown from experiments in (D). N=3 independent experiments; Student-t test (two-tail), * $p < 0.05$. Error limits are +/- SEM; Scale bars: A: 50 µm, E:100 µm.

Figure 3 ADAMTS-1 impacts *in vitro* cancer cell invasion and cell proliferation. (A) Presence of enriched ADAMTS-1 in the medium from the C.M. isolated from HEK293-T MPA strongly inhibits invasion of ES-2 cells through extracellular matrix coated filters. (B) Representative fields of views from the invasion experiments in (A). (C) Genetic deletion of ADAMTS-1 in ES-2 cells strongly enhances invasion through extracellular matrix coated filters. (D) Representative fields of views from the invasion experiments in (C). (E) Evaluation of cell proliferation and viability by the trypan blue dye exclusion method in ES-2 Wild Type and ES-2 CRISPR ADAMTS-1 cell lines treated with 10 ng / mL HGF, 10% FBS or in absence of these two factors. N=3 independent experiments; Student-t test (two-tail), ** $p < 0.01$, * $p < 0.05$. Error

limits are +/- SEM. equal symbols (*, $, #) represent statistically significant difference between groups ($p < 0.05$).

Figure 4 Deletion of ADAMTS-1 in ES-2 cells increases Src phosphorylation and relocalizes phosphorylated FAK compared to the parental ES-2 cells. Evaluation of FAK (A) and Src (B) phosphorylation in the wild-type ES-2 cells compared to the ES-2 CRISPR ADAMTS-1 cells, following serum stimulation. Evaluation of number of particles and their total area, corresponding to FAK phosphorylation (D, E), by using the thresholded image shown in (F). F, Representative immunofluorescence panels showing FAK phosphorylation following serum stimulation, in wild type ES-2 cells compared to CRISPR ADAMTS-1 cells. N=3 independent experiments; Student-t test (two-tail), * $p < 0.05$, ** $p<<0.01$. Error limits are +/- SEM. Scale bar: 5 μm. DAPI: blue; Phalloidin: green; pFAK: red.

Figure 5 Loss of ADAMTS-1 expression leads to increased and alters polarization of Cdc42 GTPase activity when compared to wild type cells. Results from the G-LISA assays are shown for Cdc42 (A, B). Serum-starved cells were stimulated with serum for 30 min prior to lysis. N=3 independent experiments; Student-t test (one-tailed), * $p < 0.05$. Error limits are +/- SEM. (C) Western blot of Cdc42 FRET biosensor expression from the stable ES-2 cell lines harboring Cdc42 FRET biosensor under tet-inducible promoter. (D) Whole-cell average Cdc42 activity levels measured using the FRET biosensor, wildtype ES-2 and the CRISPR ADAMTS-1 cell lines. n = 14 cells each, error limits are +/- SEM, * $p<0.05$ using the Student-t test (two tail). (E) Schematic depiction of the morphodynamic sampling window construction along the cell edge [33, 34]. (F and G) The evolution of the cross-correlation coefficient functions versus the timelags between edge protrusion velocity and associated Cdc42 activity fluctuations, plotted as functions of the spatial positions away from the cell edge in the ES-2 parental wildtype and CRISPR ADAMTS-1 cells responding randomly to serum, respectively. Gold and blue horizontal lines indicate p=0.05 limits (Student t-test, single-tail). Representative morphodynamic maps of the edge velocities (top) and the associated Cdc42 activity (bottom) fluctuations are shown for wildtype ES-2 cells (H) and for CRISPR ADAMTS-1 (I). Color coding: red, positive velocity of protrusion or higher Cdc42 activity; blue, negative velocity of retraction or lower Cdc42 activity.

The cutoff value of cross-correlation coefficient for significance is +/-0.18 for p=0.05 (Student t-test, single-tail), n=14 cells each condition, pooled from 5-6 independent experiments.

Figure 6 The coordination of Cdc42 activity polarizes strongly toward the leading edge in absence of ADAMTS-1, during directed migration. A, The whole-cell average Cdc42 activity levels in the control versus the CRISPR ADAMTS-1, in serum under steady-state conditions. B, The evolution of the cross-correlation coefficient functions versus the timelags between edge protrusion velocity and associated Cdc42 activity fluctuations, plotted as functions of the spatial positions away from the cell edge in the ES-2 parental wildtype cells during the wound-healing response. Gold and blue horizontal lines indicate p=0.05 limits (Student t-test, single-tail). C, Highest cross-correlation peak values are plotted as a function of the spatial positions from the leading edge, from data shown in (B). Gold dotted line indicates p=0.05 limit (Student t-test, single-tail). Asterisks indicate p<0.05. D, A schematic depiction of the regions of the highest Cdc42 activity and the edge velocity cross-correlation coefficient peaks. E, The evolution of the cross-correlation coefficient functions versus the timelags between edge protrusion velocity and associated Cdc42 activity fluctuations, plotted as functions of the spatial positions away from the cell edge in the CRISPR ADAMTS-1 cells during the wound-healing response. Gold and blue horizontal lines indicate p=0.05 limits (Student t-test, single-tail). F, Highest cross-correlation peak values are plotted as a function of the spatial positions from the leading edge, from data shown in (E). Gold dotted line indicates p=0.05 limit (Student t-test, single-tail). Asterisks indicate p<0.05. G, A schematic depiction of the regions of the highest Cdc42 activity and the edge velocity cross-correlation coefficient peaks. The cutoff value for the significance in cross-correlation coefficient is +/-0.15. n = 10 cells for the wildtype and 12 for CRISPR ADAMTS-1 cells, pooled from 5-6 independent experiments, error limits are SEM, * p<0.05. (F and G) We arbitrarily defined the index range of 1.0 to 4.0 as poorly polarized, and >4.1 as strongly polarized. F, Comparison of morphological polarity between Wild Type ES-2 and CRISPR ADAMTS-1 cells. G, Comparison of morphological polarity in ES-2 cells treated with C.M. from HEK 293-T control or MPA.

Supplementary Figure 1 Treatment of ES-2 cells with HEK 293-T MPA conditioned medium diminishes Src and FAK phosphorylation. Evaluation of FAK (A) and Src (B) phosphorylation in ES-2 cells treated with C.M. from HEK 293-T control or MPA. Quantification

of number of particles and their total area, corresponding to FAK phosphorylation (D, E), by using the thresholded image shown in (F). F, Representative immunofluorescence panels showing FAK phosphorylation following serum stimulation, in ES-2 cells treated with C.M. from HEK 293-T MPA compared to cells treated with control C.M. N=3 independent experiments; Student-t test (two-tail), *** p<<0.01. Error limits are +/- SEM. Scale bar: 5 µm. DAPI: blue; Phalloidin: green; p-FAK: red.

Supplementary Figure 2 Cdc42 activity status was not different between ES-2 cells treated with conditioned media from HEK-293T control or from that overexpressing ADAMTS-1. The whole-cell average Cdc42 levels were determined from the Cdc42 biosensor imaging (A). B) and D) The evolutions of the cross-correlation coefficient functions versus the timelags, and at different spatial positions away from the edge for the ES-2 cell lines treated with either conditioned media from the control HEK-293T or that which overexpressed ADAMTS-1. Regions above the brown line or below the blue line indicates p<0.05. C) and E) Each bar represents the peak of the cross-correlation function traces observed in (B) and (D). The cutoff value of cross-correlation coefficient for significance is +/-0.18 for p<0.05. n = 10 cells each, error limits are SEM, * p<0.05.

Supplementary Figure 3 ADAMTS-1 modulation does not alter Rac1 nor RhoA activation. Results from the G-LISA assays are shown for Rac1 with decreased or increased ADAMTS-1 (A, B) or RhoA (C,D). Serum starved cells were stimulated with serum for 30 min prior to lysis. N=3 independent experiments, Student-t test (two-tailed). Error limits are +/- SEM. WT=ES-2 wild type cells; KO=ES-2 ADAMTS-1 CRISPR cells; MPC=HEK293T Control Conditioned medium; MPA=HEK293T conditioned medium with increased ADAMTS-1.

Highlights

ADAMTS-1-enriched medium induce decrease in cell migration and invasion
CRISPR ADAMTS-1 ES-2 cells present increased migration
Decline of ADAMTS-1 enhanced the phosphorylated form of Src and FAK
Cdc42-GTP signal is significantly increased in the CRISPR ADAMTS-1 ES-2 cells.

Credit Author Statement

Maíra de Assis Lima : Conceptualization, Methodology, Writing - Original Draft

Suély Vieira da Silva Methodology, Writing - Original Draft

Orlando Serrano-Garrido Methodology

Maren Hülsemann Methodology

Luana dos Santos Neres Methodology

Juan Carlos Rodríguez-Manzaneque Methodology, Funding acquisition, Supervision.

Louis Hodgson Methodology, Writing - Review & Editing, Supervision, Funding acquisition.

Vanessa M Freitas Conceptualization, Supervision, Methodology, Project administration, Writing - Review & Editing, Funding acquisition.

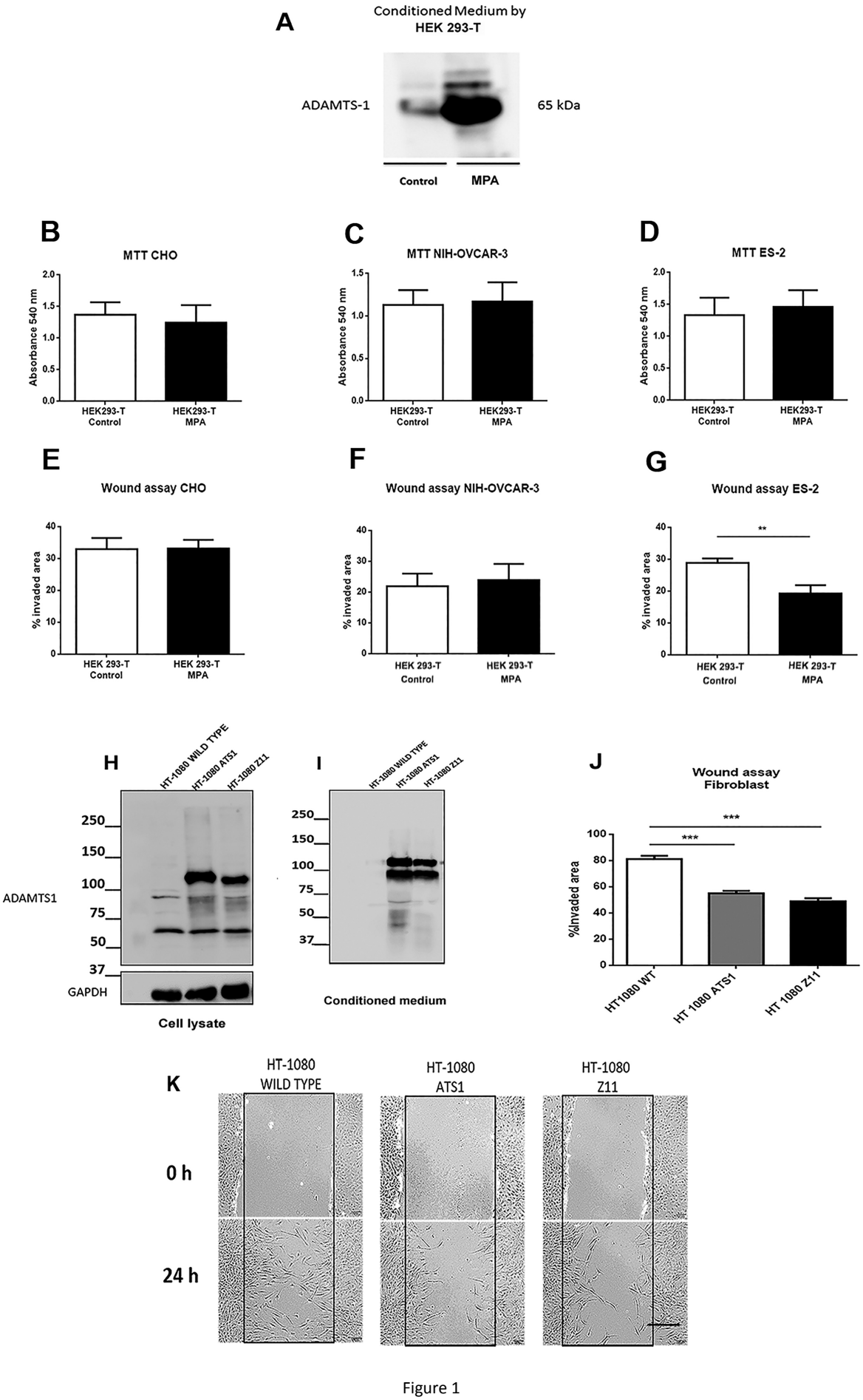
A
Conditioned Medium by HEK 293-T
ADAMTS-1
65 kDa
Control
MPA
B
MTT CHO
Absorbance 540 nm
HEK293-T Control
HEK293-T MPA
C
MTT NIH-OVCAR-3
D
MTT ES-2
E
Wound assay CHO
% invaded area
HEK 293-T Control
HEK 293-T MPA
F
Wound assay NIH-OVCAR-3
G
Wound assay ES-2
**
H
HT-1080 WILD TYPE
HT-1080 ATS1
HT-1080 Z11
ADAMTS1
GAPDH
Cell lysate
I
Conditioned medium
J
Wound assay Fibroblast
***
%Invaded area
HT1080 WT
HT 1080 ATS1
HT 1080 Z11
K
HT-1080 WILD TYPE
HT-1080 ATS1
HT-1080 Z11
0 h
24 h

Figure 1

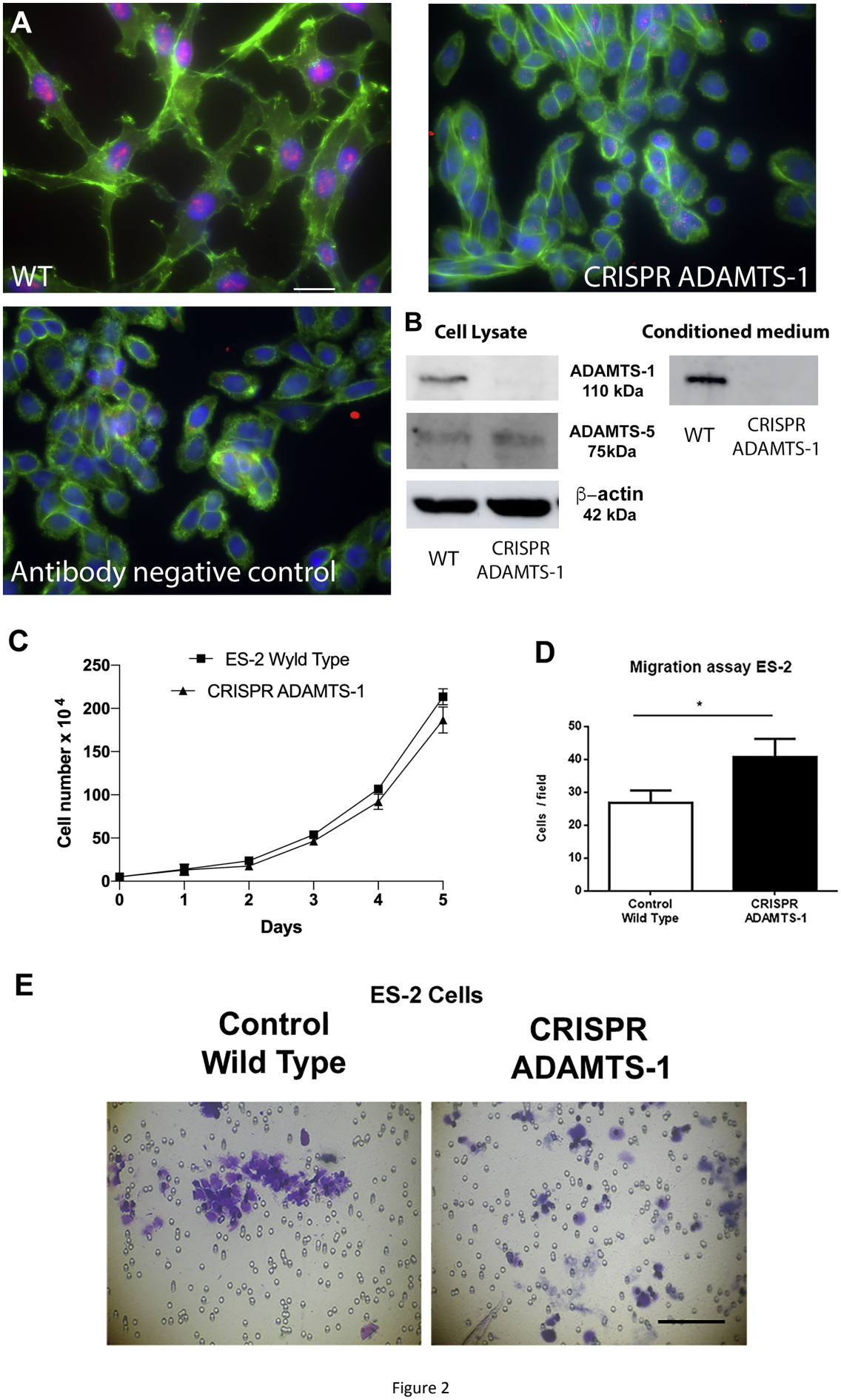
A
WT
CRISPR ADAMTS-1
Antibody negative control
B
Cell Lysate
Conditioned medium
ADAMTS-1
110 kDa
ADAMTS-5
75kDa
β–actin
42 kDa
WT
CRISPR
ADAMTS-1
WT
CRISPR
ADAMTS-1
C
ES-2 Wyld Type
CRISPR ADAMTS-1
Cell number x 10 4
250
200
150
100
50
0
0
1
2
3
4
5
Days
D
Migration assay ES-2
*
Cells / field
50
40
30
20
10
0
Control
Wild Type
CRISPR
ADAMTS-1
E
ES-2 Cells
Control
Wild Type
CRISPR
ADAMTS-1

Figure 2

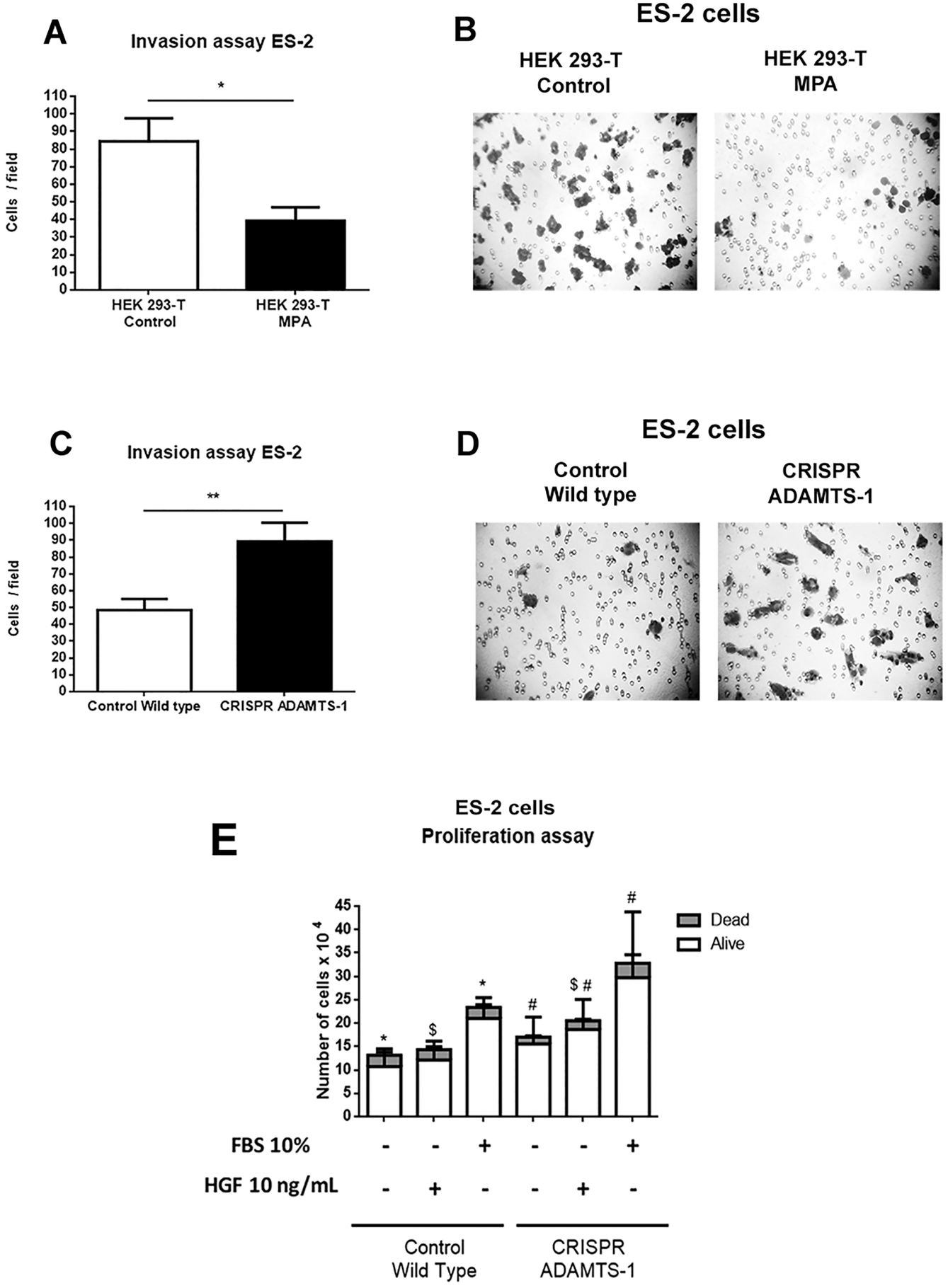
A
Invasion assay ES-2
Cells / field
HEK 293-T Control
HEK 293-T MPA
B
ES-2 cells
HEK 293-T Control
HEK 293-T MPA
C
Invasion assay ES-2
Cells / field
Control Wild type
CRISPR ADAMTS-1
D
ES-2 cells
Control Wild type
CRISPR ADAMTS-1
E
ES-2 cells
Proliferation assay
Number of cells x 10 4
Dead
Alive
FBS 10%
HGF 10 ng/mL
Control Wild Type
CRISPR ADAMTS-1

Figure 3

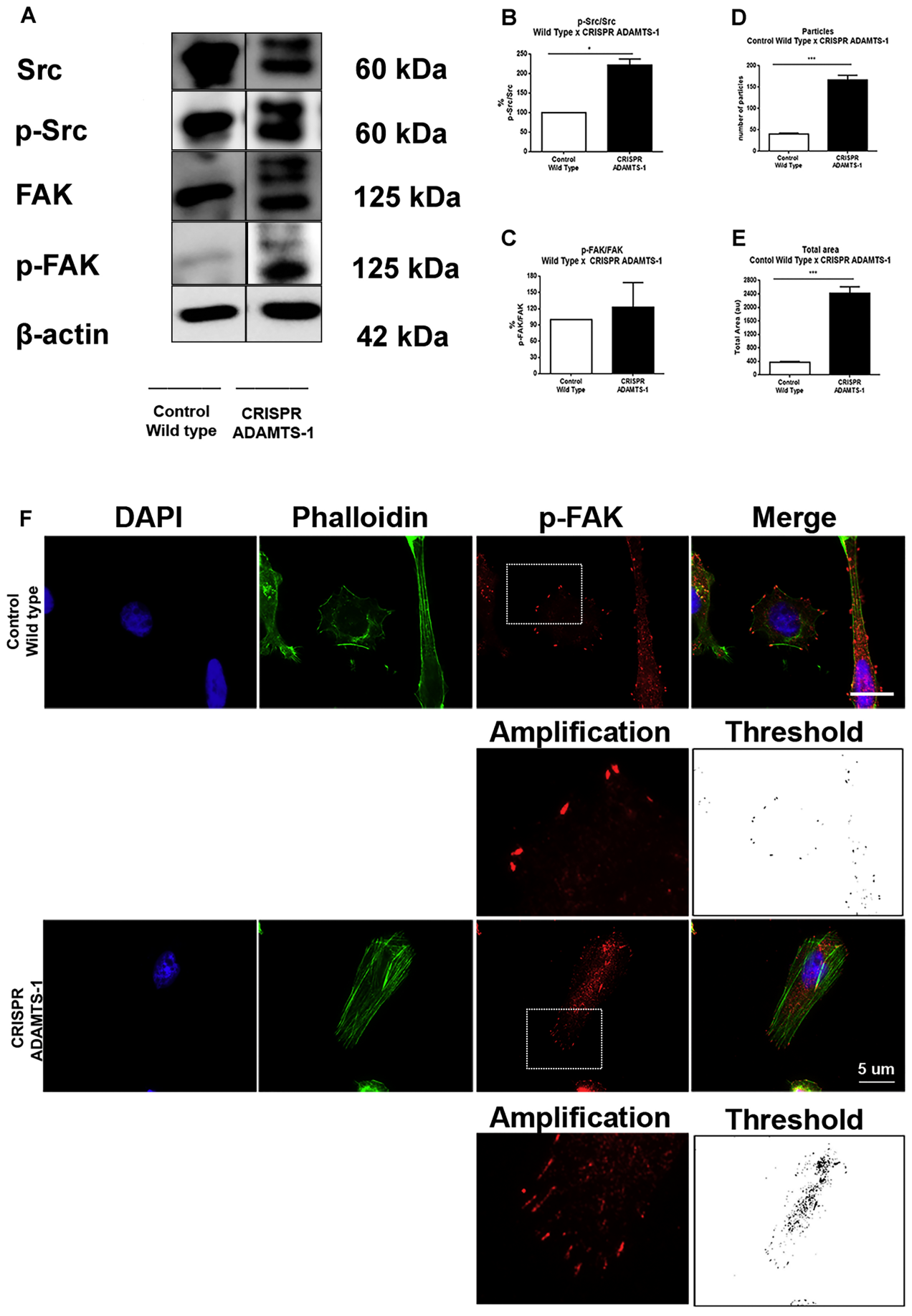
A
Src
p-Src
FAK
p-FAK
β-actin
60 kDa
60 kDa
125 kDa
125 kDa
42 kDa
Control Wild type
CRISPR ADAMTS-1
B
p-Src/Src
Wild Type x CRISPR ADAMTS-1
% p-Src/Src
Control Wild Type
CRISPR ADAMTS-1
C
p-FAK/FAK
Wild Type x CRISPR ADAMTS-1
% p-FAK/FAK
D
Particles
Control Wild Type x CRISPR ADAMTS-1
number of particles
E
Total area
Contol Wild Type x CRISPR ADAMTS-1
Total Area (au)
F
DAPI
Phalloidin
p-FAK
Merge
Control Wild type
Amplification
Threshold
CRISPR ADAMTS-1
5 um

Figure 4

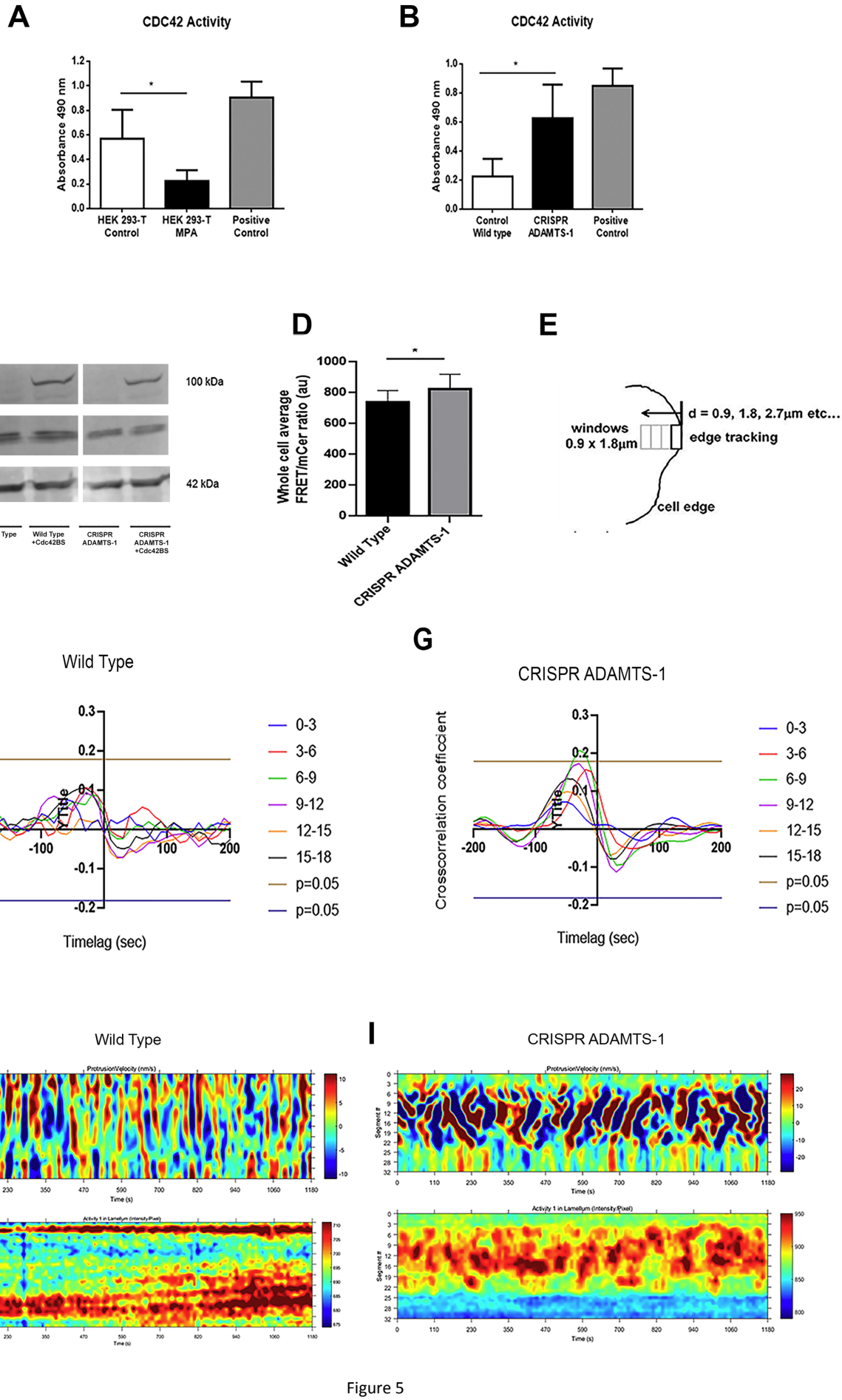
A
CDC42 Activity
Absorbance 490 nm
HEK 293-T Control
HEK 293-T MPA
Positive Control
B
CDC42 Activity
Absorbance 490 nm
Control Wild type
CRISPR ADAMTS-1
Positive Control
C
Cdc42 Biosensor
Total Cdc42
Actin
100 kDa
42 kDa
Wild Type
Wild Type +Cdc42BS
CRISPR ADAMTS-1
CRISPR ADAMTS-1 +Cdc42BS
D
Whole cell average FRET/mCer ratio (au)
Wild Type
CRISPR ADAMTS-1
E
d = 0.9, 1.8, 2.7µm etc...
windows 0.9 x 1.8µm
edge tracking
cell edge
F
Wild Type
Crosscorrelation coefficient
Timelag (sec)
0-3
3-6
6-9
9-12
12-15
15-18
p=0.05
p=0.05
G
CRISPR ADAMTS-1
Crosscorrelation coefficient
Timelag (sec)
0-3
3-6
6-9
9-12
12-15
15-18
p=0.05
p=0.05
H
Wild Type
Protrusion Velocity (nm/s)
Segment #
Time (s)
Activity 1 in Lamellum (Intensity/Pixel)
I
CRISPR ADAMTS-1
Protrusion Velocity (nm/s)
Segment #
Time (s)
Activity 1 in Lamellum (Intensity/Pixel)

Figure 5

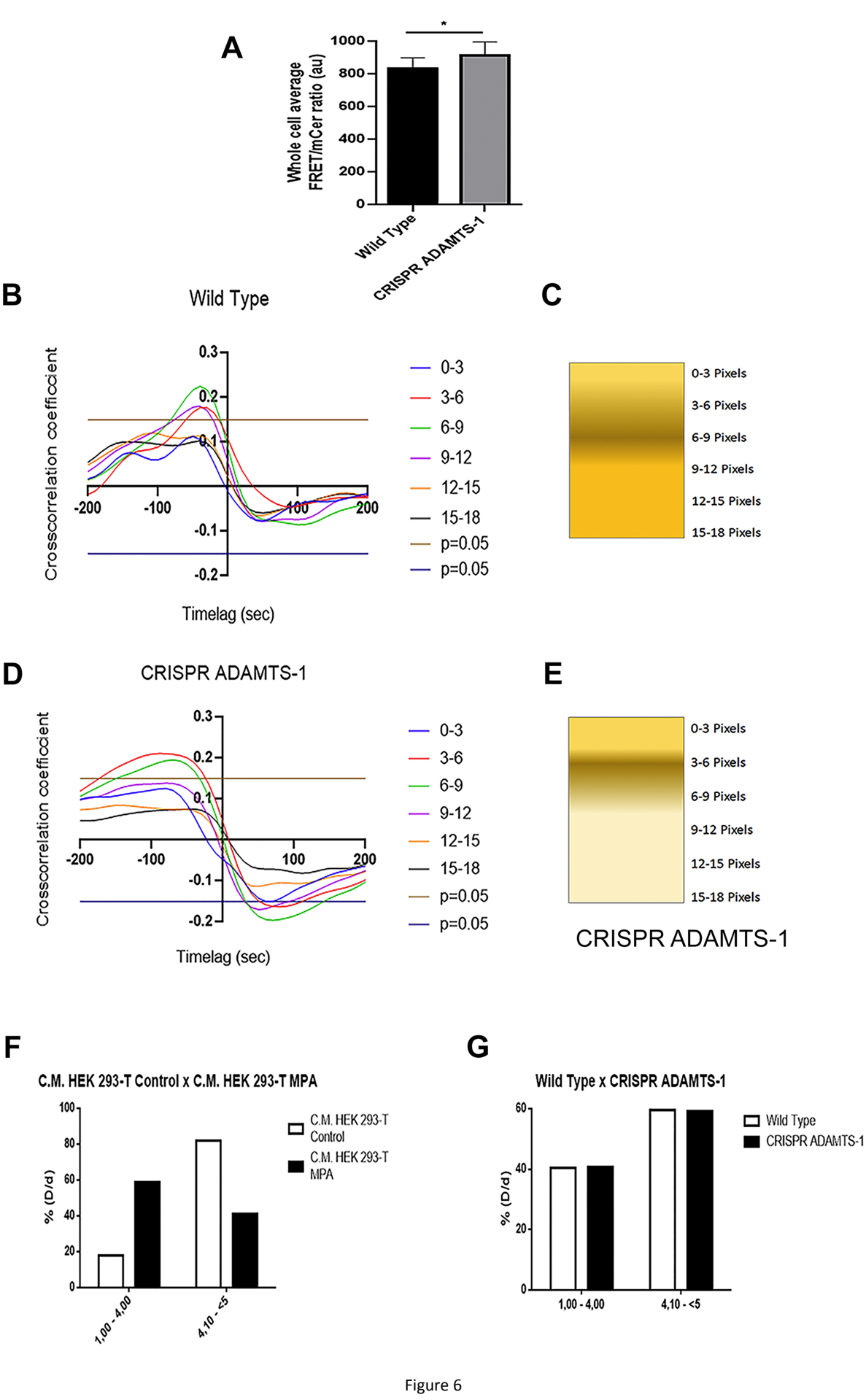
A
Whole cell average FRET/mCer ratio (au)
1000
800
600
400
200
0
*
Wild Type
CRISPR ADAMTS-1
B
Wild Type
Crosscorrelation coefficient
0.3
0.2
0.1
-0.1
-0.2
-200
-100
100
200
Timelag (sec)
0-3
3-6
6-9
9-12
12-15
15-18
p=0.05
p=0.05
C
0-3 Pixels
3-6 Pixels
6-9 Pixels
9-12 Pixels
12-15 Pixels
15-18 Pixels
D
CRISPR ADAMTS-1
Crosscorrelation coefficient
Timelag (sec)
0-3
3-6
6-9
9-12
12-15
15-18
p=0.05
p=0.05
E
0-3 Pixels
3-6 Pixels
6-9 Pixels
9-12 Pixels
12-15 Pixels
15-18 Pixels
CRISPR ADAMTS-1
F
C.M. HEK 293-T Control x C.M. HEK 293-T MPA
% (D/d)
100
80
60
40
20
0
C.M. HEK 293-T Control
C.M. HEK 293-T MPA
1,00 - 4,00
4,10 - <5
G
Wild Type x CRISPR ADAMTS-1
% (D/d)
60
40
20
0
Wild Type
CRISPR ADAMTS-1
1,00 - 4,00
4,10 - <5

Figure 6